Received November 2003
Revised October 2004
Accepted February 2005

Quadratic Petrov-Galerkin finite elements for advective-reactive features in turbomachinery CFD

Alessandro Corsini, Franco Rispoli and Andrea Santoriello
Department of Mechanics and Aeronautics, University of Rome "La Sapienza", Roma, Italy

Abstract

Purpose – An original finite element scheme for advection-diffusion-reaction problems is presented. The new method, called spotted Petrov-Galerkin (SPG), is a quadratic Petrov-Galerkin (PG) formulation developed for the solution of equations where either reaction (associated to zero-order derivatives of the unknown) and/or advection (proportional to first-order derivatives) dominates on diffusion (associated to second-order derivatives). The addressed issues are turbulence and advective-reactive features in modelling turbomachinery flows.

Design/methodology/approach – The present work addresses the definition of a new PG stabilization scheme for the reactive flow limit, formulated on a quadratic finite element space of approximation. We advocate the use of a higher order stabilized formulation that guarantees the best compromise between solution stability and accuracy. The formulation is first presented for linear scalar one-dimensional advective-diffusive-reactive problems and then extended to quadrangular Q2 elements.

Findings – The proposed advective-diffusive-reactive PG formulation improves the solution accuracy with respect to a standard streamline driven stabilization schemes, e.g. the streamline upwind or Galerkin, in that it properly accounts for the boundary layer region flow phenomena in presence of non-equilibrium effects.

Research limitations/implications – The numerical method here proposed has been designed for second-order quadrangular finite-elements. In particular, the Reynolds-Averaged Navier-Stokes equations with a non-linear turbulence closure have been modelled using the stable mixed element pair Q2-Q1.

Originality/value – This paper investigated the predicting capabilities of a finite element method stabilized formulation developed for the purpose of solving advection-reaction-diffusion problems. The new method, called SPG, demonstrates its suitability in solving the typical equations of turbulence eddy viscosity models.

Keywords Finite element analysis, Galerkin method, Turbulent flow

Paper type Research paper

Introduction

In this work, we focus on the numerical solution of advection-diffusion-reaction problems using the finite element method (FEM) on quadratic spaces of approximation. Here, diffusion, advection and reaction refer to those terms in the partial differential equations (PDEs) involving second-, first- and zero-order derivatives of the unknown. This family of equations, that governs several phenomena of industrial interest, is

The authors acknowledge MIUR under the projects URLS-Ateneo 2002, and High Performance Computing Grant 2003.

International Journal of Numerical Methods for Heat & Fluid Flow
Vol. 15 No. 8, 2005
pp. 894-925

0961-5539
DOI 10.1108/09615530510625147

considered here because of its importance in the turbulence modelling for turbomachinery computational fluid dynamics (CFD). Concerning the solution of PDEs for incompressible flows, the use of standard schemes, such as central finite differences or Galerkin finite elements, features several sources of oscillations. Since the appearance in the early 1980s of the first works by Hughes and Brooks (1982a, b), the main recognised shortcoming of symmetric numerical schemes was the lack of stability in presence of particular flow conditions, such as advection dominated flows or sharp boundary layers. In the finite element framework, stabilized formulations have been proposed during the last two decades as remedial strategies. The Petrov-Galerkin (PG) approach has been widely used to build-up consistent residual-based stabilization devices. To mention but a few, in the advective limit the test functions are sensitised by asymmetric streamwise perturbations (e.g. streamline upwind or Galerkin (SUPG) schemes in Hughes and Brooks, 1982a, b; Tezduyar *et al.*, 1992; Codina *et al.*, 1992), or in the diffusive limit the Babuska-Brezzi condition is circumvented making the perturbation proportional to the momentum residual (e.g. PSPG scheme in Tezduyar *et al.*, 1992). A different approach effective in controlling advection induced wiggles makes use of the concept of residual free bubbles (Brezzi *et al.*, 1998).

Moving towards turbomachinery CFD, an additional origin of numerical deficiencies stems from the reaction or zero-order derivative terms. These terms are usually related to the rotation of turbomachinery frame of reference (e.g. in the modelling of Coriolis forces), but they also appear in the turbulence closure equations (e.g. two equations eddy viscosity models). In this ambit, they are related to dissipation terms and play a critical role in the development of boundary layers in the case of vanishing advection effects, such as in the transitional region, or in the stagnation and separation flow cores. Whenever the reaction is present, local oscillations, near boundaries or solution discontinuities, may be originated but they typically do not degrade the global solution accuracy (Codina, 2001). As a matter of fact, in this case it is not possible to obtain a global stability estimate in the H^1 norm, though it could be evaluated in L^2, thus explaining the local scale of the oscillations.

To the best of the authors' knowledge, most of the formulations proposed for advective-diffusive-reactive flow problems have been designed for linear equations and linear elements, such as the (SU + C)PG by Idelsohn *et al.* (1996) or the GGLS by Harari and Hughes (1994). Only few works concern with reactive problems pertinent to turbomachinery fluid dynamics (Codina and Soto, 1997).

In this viewpoint, the present work addresses the definition of a new PG stabilization scheme for the reactive flow limit, formulated on a quadratic finite element space of approximation. We advocate the use of a higher order stabilized formulation (despite of its coding complexity, due to non-negligible second-order derivatives) that guarantees the best compromise between solution stability and accuracy (Borello *et al.*, 2003). The proposed method, called spotted Petrov-Galerkin (SPG), possesses some distinctive features. For advection-diffusion problems it behaves like a SUPG method, whereas in the reactive-diffusive limit it turns to a space invariant perturbation able to give rise to spot-like weight functions, symmetric and concentrated around each nodal position. In intermediate situations, the scheme combines the advective and reactive perturbation integrals using nodal tuning or upwind coefficients that depend on element Peclet and reaction numbers and are

designed to circumvent any compounding effect. The multi-dimensional variant of the SPG method has been used on linear PDEs and on the Reynolds Averaged Navier-Stokes (RANS) equations in combination with two equations k-ε models, both standard (Launder and Sharma, 1974) and non-linear variants (Craft *et al.*, 1996).

The remainder of the paper is organised as follows. First, the Galerkin formulation of the general advective-diffusive-reactive problem is presented. In order to show the instability origin for reaction-dominated problems, we then consider a one-dimensional (1D) problem in the null advection limit, addressing the need for a stabilized numerical scheme. Then the SPG formulation is presented for the linear scalar 1D advective-diffusive-reactive equation. The extension of the formulation to the multi-dimensional case is discussed, and the family of weights for quadrangular Q2 element is shown. Then the whole stabilized SPG formulation for the RANS approach to incompressible turbulent flows is presented, commenting on the reactivity features arising in the closure equations of turbulence EVMs. Finally, the performance of SPG are assessed against solutions provided by SUPG, both for model problems and for real turbulent flow configurations.

Finite element scalar advective-diffusive-reactive problem; reaction induced instabilities

Let us take the general linear scalar advective-reactive-diffusive problem statement on the closed domain $\underline{\Omega}$ for the unknown U:

$$F_a(U)_{,j} + F_d(U, \nabla U)_{,j} + F_r(U) = f \quad \text{in } \Omega \in \mathbb{R}^{\text{nsd}} \tag{1.1}$$

$$U(\Gamma_D) = U_{\text{D}}$$
$$U_{,n}(\Gamma_N) = \theta_{\text{N}}$$

where nsd is the number of space dimensions and the structure of the operators reads as:

$$\begin{aligned} F_a(U) &= u_j U \\ F_d(U, \nabla U) &= -kU_{,j} \\ F_r(U) &= cU \end{aligned} \tag{1.2}$$

and u_j are the solenoidal velocity components, $k > 0$ is the constant diffusivity, $c \geq 0$ is the reaction coefficient and f the source term. The boundary conditions are specified along the surface boundary $\Gamma = \underline{\Gamma}_N \cup \underline{\Gamma}_D$ ($\underline{\Gamma}_N$ and $\underline{\Gamma}_D$ are closed, disjoint subsets of Γ), including Dirichlet (U_{D}) and Neumann conditions (θ_{N}).

Given a finite element partition of the original closed domain $\underline{\Omega}$ into elements Ω_e, $e = 1$, nel (nel, number of elements), such that:

$$\cup_e \Omega_e = \Omega \quad \text{and} \quad \cap_e \Omega_e = \varnothing \tag{2.1}$$

with the interior boundaries:

$$\Gamma_{\text{int}} = \cup_e \Gamma_e - \Gamma \tag{2.2}$$

Let define the finite dimensional spaces of trial and weight functions as:

$$S^h = \left\{ U^h | U^h \in H^{1h}(\Omega), U^h = U_{\mathrm{D}} \text{ on } \Gamma_D, U_{\mathrm{D}} \in H^{(1/2)h}(\Gamma_D) \right\} \tag{3.1}$$

$$W^h = \left\{ w^h | w^h \in H_0^{1h}, w^h = 0 \text{ on } \Gamma_D \right\} \tag{3.2}$$

where $H^{1h}(\Omega)$ and $H_0^{1h}(\Omega)$ are the Sobolev spaces for the continuous pair of finite element functions, $H^{(1/2)h}(\Gamma_D)$ is their restriction to the domain boundary, and the superscript h denotes the characteristic length scale of the domain discretization. The Galerkin weak formulation of problem (1.1) and (1.2) reads as follows:

$$\begin{aligned} &\sum_{e=1}^{\mathrm{nel}} \int_{\Omega_e} w^h F_{a,j}^h \, \mathrm{d}\Omega - \sum_{e=1}^{\mathrm{nel}} \int_{\Omega_e} w_{,j}^h F_d^h \, \mathrm{d}\Omega \\ &+ \sum_{e=1}^{\mathrm{nel}} \int_{\Omega_e} w^h F_r^h \, \mathrm{d}\Omega = \sum_{e=1}^{\mathrm{nel}} \int_{\Omega_e} w^h f \, \mathrm{d}\Omega + \int_{\Gamma_N} w^h k \frac{\partial U^h}{\partial n} \, \mathrm{d}\Gamma \end{aligned} \tag{4}$$

The solution obtained with equation (4) for advection dominated problems is affected by spurious oscillations, that could be tackled with stabilized formulations such as SUPG. Also reaction terms give rise to oscillations that must be controlled by means of stabilized formulations enriched with built-in components to preclude oscillatory behaviour in the reaction-dominated limit. In this viewpoint, let us consider the ordinary differential equation obtained from equations (1.1) and (1.2), for $\mathrm{nsd} = 1$, and source term $f = 0$:

$$u \frac{\mathrm{d}U}{\mathrm{d}x} - k \frac{\mathrm{d}^2 U}{\mathrm{d}x^2} + cU = 0 \tag{5}$$

The discretization of equation (5), for constant physical properties, using the Galerkin method on a quadratic space of interpolation, with uniform element of length h, gives rise to the following difference equations:

$$U_{i-1}[-4 - 2Pe + r/10] + U_i[8 + r4/5] + U_{i+1}[-4 + 2Pe + r/10] = 0 \tag{6}$$

for (i) element central node, and

$$\begin{aligned} &U_{i-2}[1 + Pe - r/10] + U_{i-1}[-8 - 4Pe + r/5] + U_i[14 + r4/5] \\ &\quad + U_{i+1}[-8 + 4Pe + r/5] + U_{i+2}[1 - Pe - r/10] = 0 \end{aligned} \tag{7}$$

for $(i-2, i, i+2)$ element extreme nodes.

In the above equations, the magnitudes of advection or reaction versus diffusion are given by the element Peclet number $Pe = \|u\|h/2k$, and the element reaction number $r = ch^2/k$, respectively.

In order to have a first insight on the instability origin of the reaction dominated case, let now consider the null advection limit of the studied problem, focusing, for instance, on element central nodes. In this case, equation (6) turns to the following expression:

$$U_{i-1}[-4+r/10]+U_i[8+r4/5]+U_{i+1}[-4+r/10]=0 \tag{8}$$

The solutions of the characteristic equation associated to equation (8), the so-called Galerkin nodal amplification factors (Harari and Hughes, 1994), purely depend on the magnitude of reaction:

$$\rho=\frac{-\left(8+\frac{4}{5}r\right)\pm\sqrt{\left(8+\frac{4}{5}r\right)^2-4\left(-4+\frac{r}{10}\right)^2}}{2\left(-4+\frac{r}{10}\right)} \tag{9}$$

The influence exerted on ρ shows that the exact solution exponential behaviour is preserved only with $r<40$. This circumstance confirms the need of designing a stabilized scheme with built-in component to preclude oscillatory behaviour in reaction dominated cases.

SPG formulation

The stabilized SPG formulation is obtained by imposing nodal exactness to the numerical solution of problem (5). Provided that different equations have been obtained for the extreme and central nodes (Codina *et al.*, 1992), it is possible to find two optimal modified weights, on the basis of the discrete equations (6) and (7) separately. Each of these resulting PG weight functions is obtained from the addition to the Galerkin one w_i (for the sake of simplicity, from now on the superscript h that denotes the finite dimensional spaces of weight and trial functions will be omitted) of two perturbation functions, the first one to control advection induced oscillations and the second for reaction induced ones (as first suggested for linear elements by Idelsohn *et al.*, 1996), and for each element node (i) read as:

$$\tilde{w}_i=w_i+\zeta_{a_i}P_{a_i}+\zeta_{r_i}P_{r_i} \tag{10}$$

where ζ_{a_i} and ζ_{r_i}, the tuning coefficients for the two perturbation functions, respectively, P_{a_i} for advection induced instabilities and P_{r_i} for reaction induced ones.

The first perturbation is formally similar to a SUPG one and reads as:

$$P_{a_i}=\frac{h}{2\|u\|}u_k w_{i,k} \tag{11}$$

On the other hand, the design of the perturbation function that controls reaction effects is based on the following constraints. First, in the null advection case the invariance of the equation under coordinate inversion suggests to adopt symmetric weight $\tilde{w}_i$ (Idelsohn *et al.*, 1996). Moreover, in the pure reaction limit ($r\rightarrow\infty$), the optimal weight would be a Dirac's delta. On this basis, the perturbation suggested by the authors is a symmetric and negative definite polynomial (Idelsohn *et al.*, 1996), and must fulfil at least six constraints, i.e. it must be zero with zero first-order derivative on the element nodes. The lowest order polynomial with these features is a sixth-order one; the seventh constraint imposed by the authors is represented by the C_{SPG} value which sets the magnitude of the weight reduction between two neighbouring nodes:

$$P_{r_i}=P_r=-\frac{C_{\mathrm{SPG}}}{l_\xi^6}\left[\xi^6-\frac{l_\xi^2}{2}\xi^4+\frac{l_\xi^4}{16}\xi^2\right] \tag{12}$$

where ξ represents the coordinate in the master or logic space and l_ξ its dimension (in our case equal to 2). It is remarkable that the periodic-like behaviour of this function permits to use the same analytical expression for each node. The coefficient C_{SPG} is used to set the asymptotic values of the tuning functions ζ_{r_i}, without affecting ζ_{a_i}.

The expression for the tuning functions are consequent to the super-convergence condition (Codina *et al.*, 1992; Idelsohn *et al.*, 1996) that requires the identity between the discrete and the exact solution in case of a homogeneous linear 1D problem. In particular, the use of the SPG method to solve equation (5) on a quadratic space of interpolation, with uniform elements of length h, gives rise to the following difference equations:

$$-a_6 \cdot U_{i-1} + d_8 \cdot U_i - a_7 \cdot U_{i+1} = 0 \tag{13.1}$$

for (i) element central node, and

$$\begin{aligned} &U_{i-2}[a_2 + b_2\zeta_{a_1} + e_2\zeta_{r_1}] + U_{i-1}[a_1 + b_1\zeta_{a_1} + e_1\zeta_{r_1}] + U_i[a_4 + b_4\zeta_{a_1} + e_4\zeta_{r_1}] \\ &\quad + U_{i+1}[a_3 + b_3\zeta_{a_1} + e_3 4.55\zeta_{r_1}] + U_{i+2}[a_5 + b_5\zeta_{a_1} + e_5\zeta_{r_1}] = 0 \end{aligned} \tag{13.2}$$

for $(i-2, i, i+2)$ element extreme nodes. It should be remarked that in equation (13.1) the coefficients are linear function of the unknowns, namely ζ_{a_2}, ζ_{r_2}, and equation (13.2) provides $\zeta_{a_1} = \zeta_{a_3}, \zeta_{r_1} = \zeta_{r_3}$. Equations (13.1) and (13.2) are written in a synthetic way, and the complete expressions of the coefficients are given in Appendix 1.

The substitution of the analytical solution into equations (13.1) and (13.2), permits to obtain first ζ_{a_2}, ζ_{r_2} and as a consequence ζ_{a_1}, ζ_{r_1}. For the sake of completeness the analytical expressions of the tuning functions are summarized in Appendix 2.

Figure 1 shows the perturbed weight function $\tilde{w}_i$, for 1D quadratic elements in case of null advection with varying tuning coefficients ζ_{r_i}, both for central and extreme nodes. The weights are plotted for $C_{\mathrm{SPG}} = (2^{12}/3^2) \times 0.35$. This value stems from the fulfilment of seven constraints for the P_r perturbation on quadratic elements, including: null nodal values and derivatives, P_r intensity at $\xi = \pm l_\xi/4$.

Figure 2(a) shows the behaviours of ζ_{a_i} for different combinations of Pe and r. Furthermore, Figure 2(b) shows that of ζ_{r_i} tuning functions.

It is remarkable that the sensitivity to the reactive part of the differential operator gives rise to the tuning functions ζ_{r_i} and the behaviour of the formulation in the null-reaction limit approaches the SUPG Q2 one proposed by Codina *et al.* (1992).

Extension of SPG formulation to multi-dimensional case

The two-dimensional (2D) extension of the P_r function is designed to preserve its 1D requirement, that is the isotropic concentration of the perturbed weight around the nodal positions. To this end, we designed a Cartesian product between the 1D counterparts of the second perturbation function, where the P_r spots are moved in the element portion closer to the corresponding nodes. This concept is depicted in Figure 3 that shows the resulting geometries for the 2D second perturbation functions on logic space. In such a way, it is possible to maintain the continuity of the P_r on the inter-element boundary.

It is worth noting that the 2D tuning functions ζ_{r_i} are obtained on the basis of a pure positional criterion on logic space. For example, in the case of the mid-side node of Figure 3(c) the tuning function is a linear combination of ζ_{r_1} and ζ_{r_2}.

RANS formulation in presence of reaction

Fluid model formulation

The dynamic response of incompressible turbulent flows is modelled by using a RANS approach. Each quantity **U** is then decomposed into its conventional average (denoted by an overbar) and the fluctuation with respect to the latter (denoted by a prime), as $\boldsymbol{U} = \overline{\boldsymbol{U}} + \boldsymbol{U}'$. In the present work, it is used a cubic k-ε model (Craft *et al.*, 1996), labelled CLS96. The non-isotropic constitutive relation for the Reynolds stresses $\rho\overline{u_i' u_j'}$ is in the form of a third-order polynomial of the mean strain and vorticity tensors, and scalar turbulent viscosity ν_t:

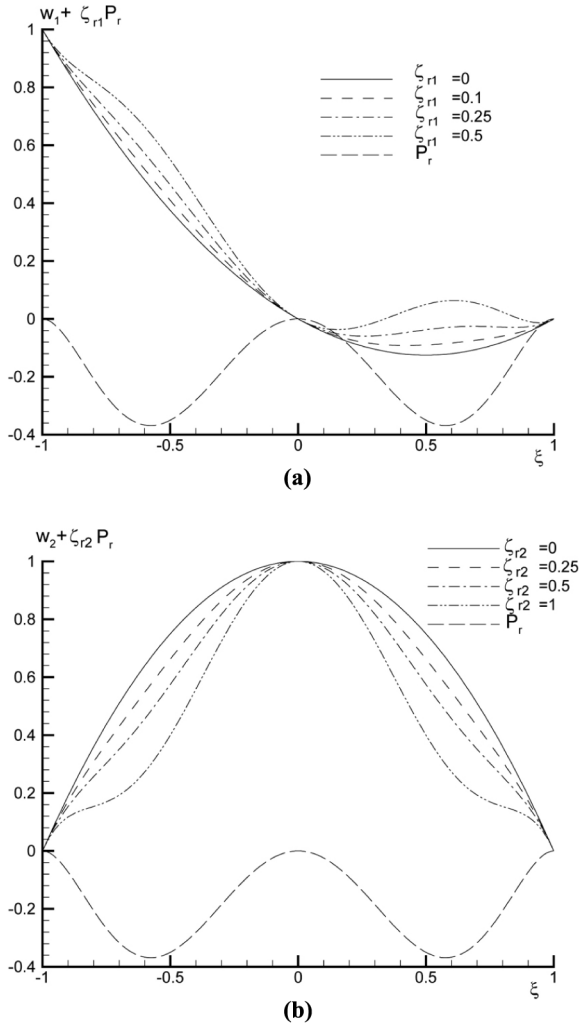

Figure 1.
1D null advection: (a) resulting weight for extreme node; and (b) for central node

$$\overline{u_i' u_j'} = \frac{2}{3}k\delta_{ij} - \nu_t S_{ij} + -0.1\nu_t \frac{k}{\varepsilon}\left(S_{ik}S_{kj} - S_{kl}S_{kl}\frac{1}{3}\delta_{ij}\right) + 0.1\nu_t \frac{k}{\varepsilon}(W_{ik}S_{kj} + W_{jk}S_{ki})$$
$$+ 0.26\nu_t \frac{k}{\varepsilon}\left(W_{ik}W_{kj} - W_{kl}W_{kl}\frac{1}{3}\delta_{ij}\right) - 10c_\mu^3 \nu_t \left(\frac{k}{\varepsilon}\right)^2 (S_{ki}W_{lj} + S_{kj}W_{li})S_{kl} \quad (14)$$
$$- 5c_\mu^3 \nu_t \left(\frac{k}{\varepsilon}\right)^2 S_{ij}S_{kl}S_{kl} + 5c_\mu^3 \nu_t \left(\frac{k}{\varepsilon}\right)^2 S_{ij}W_{kl}W_{kl}$$

where $S_{ij} = (\bar{u}_{i,j} + \bar{u}_{j,i})$ is twice the strain tensor, $W_{ij} = (\bar{u}_{i,j} - \bar{u}_{j,i})$ is twice the vorticity tensor, and δ_{ij} is the Kronecker tensor. The turbulent viscosity is defined as:

$$\nu_t = c_\mu f_\mu \frac{k^2}{\varepsilon} \quad (15.1)$$

with

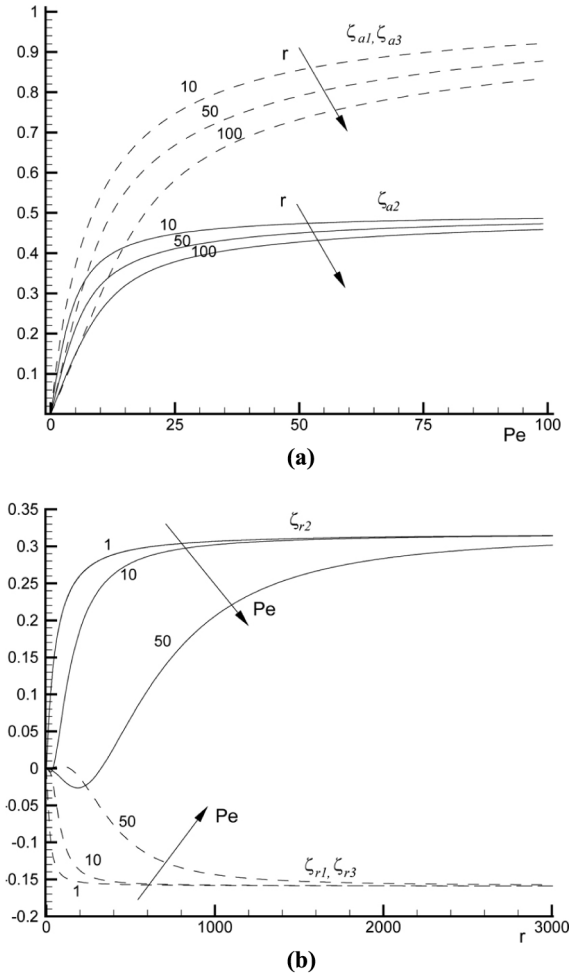

Figure 2.
SPG tuning functions

$$c_\mu = \frac{0.3[1 - \exp[-0.36/\exp[-0.75\max(S, W)]]]}{1 + 0.35[\max(S, W)]^{1.5}} \tag{15.2}$$

$$f_\mu = 1 - \exp\left[-\left(\frac{Re_t}{90}\right)^{0.5} - \left(\frac{Re_t}{400}\right)^2\right] \tag{15.3}$$

where $Re_t = k^2/\nu\varepsilon$ is the turbulence Reynolds number, S and W are, respectively, the strain and vorticity invariants defined as:

$$S = \frac{k}{\varepsilon}\sqrt{\frac{1}{2}S_{ij}S_{ij}} \quad W = \frac{k}{\varepsilon}\sqrt{\frac{1}{2}W_{ij}W_{ij}} \tag{15.4}$$

As shown by the validation studies presented by Chen and Leschziner (1999) and Corsini and Rispoli (2002), the stress-strain cubic dependence is a mean to establish an appropriate sensitivity to streamline curvature. The non-isotropic model is coupled with a two-equations closure, where the turbulent velocity- and length-scales are determined by solving steady-state conservation equations for the turbulent kinetic energy and the isotropic turbulent dissipation.

Problem statement

The complete RANS formulation is obtained in terms of: the momentum components $\rho\bar{u}_i (i = 1, 2, 3)$ (where ρ is the density, and $\bar{u}_i$ the Cartesian averaged velocity components), the static pressure $\overline{p}$, the turbulent kinetic energy k, and the dissipation variable $\tilde{\varepsilon} = \varepsilon - 2\nu(\partial\sqrt{k}/\partial x_i)^2$, that replaces the isotropic dissipation rate ε.

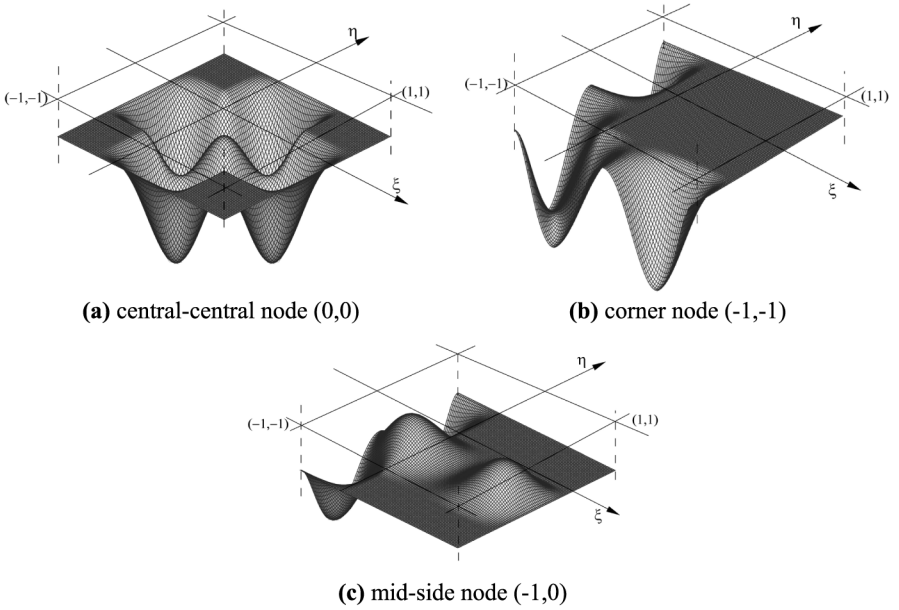

(a) central-central node (0,0)

(b) corner node (-1,-1)

(c) mid-side node (-1,0)

Figure 3.
2D P_r functions in the logic space

The boundary value problem reads as:

$$\begin{aligned} &F_a(\tilde{\boldsymbol{U}})_j + F_d(\tilde{\boldsymbol{U}}, \nabla\tilde{\boldsymbol{U}})_j - \rho f = 0 \ \text{ in } \ \Omega \in \mathbb{R}^{\text{nsd}} \\ &\overline{\boldsymbol{U}} = \overline{\boldsymbol{U}}_{\text{D}} \ \text{ on } \ \Gamma_D \\ &F_{d,n} = \theta_{\text{N}} \ \text{ on } \ \Gamma_N \end{aligned} \tag{16}$$

where $\overline{\boldsymbol{U}}$ is the vector of the averaged unknowns related to $\tilde{\boldsymbol{U}}$ by:

$$\overline{\boldsymbol{U}} \equiv \left[\bar{u}_1, \quad \bar{u}_2, \quad \bar{u}_3, \quad \bar{p}, \quad k, \quad \tilde{\varepsilon}\right]^{\text{T}} = \tilde{\boldsymbol{U}} + \left[0, \quad 0, \quad 0, \quad \bar{p} - 1, \quad 0, \quad 0\right]^{\text{T}} \tag{17}$$

which could be interpreted in terms of the primary-turbulent flow properties

$$\overline{\boldsymbol{U}}_p \equiv [\,\bar{u}_1, \quad \bar{u}_2, \quad \bar{u}_3, \quad 0, \quad k, \quad \tilde{\varepsilon}\,]^{\text{T}}$$

and of the constrained variables

$$\overline{\boldsymbol{U}}_c \equiv [\,0, \quad 0, \quad 0, \quad \bar{p}, \quad 0, \quad 0\,]^{\text{T}}.$$

The boundary conditions, specified along the computational domain boundary, generally include inflow Dirichlet conditions ($\overline{\boldsymbol{U}}_{\text{D}}$) and outflow Neumann conditions (θ_{N}). On solid boundaries, homogeneous Dirichlet conditions are imposed for $\overline{\boldsymbol{U}}_p$.

The flux vectors appearing in equation (16) are defined as:

$$F_a(\tilde{\boldsymbol{U}}) = [\bar{u}_j\rho\bar{u}_1, \bar{u}_j\rho\bar{u}_2, \bar{u}_j\rho\bar{u}_3, \bar{u}_j, \bar{u}_j\rho k, \bar{u}_j\rho\tilde{\varepsilon}]^{\text{T}} \tag{18.1}$$

$$F_d(\tilde{\boldsymbol{U}}, \nabla\tilde{\boldsymbol{U}}) = \left[\bar{\sigma}_{1j}, \bar{\sigma}_{2j}, \bar{\sigma}_{3j}, 0, -\rho\left(\nu + \frac{\nu_{\text{t}}}{\sigma_k}\right)k_{,j}\,, -\rho\left(\nu + \frac{\nu_{\text{t}}}{\sigma_\varepsilon}\right)\tilde{\varepsilon}_{,j}\right]^{\text{T}} \tag{18.2}$$

where the stress tensor is:

$$\bar{\sigma}_{ij} = \bar{p}^*\,\delta_{ij} - \rho(\nu + \nu_{\text{t}})(\bar{u}_{i,j} + \bar{u}_{j,i}) \tag{18.3}$$

The non-linear Newtonian like turbulent stress terms are thus included, adding ν_{t} to the molecular kinematic viscosity, whereas the modified pressure ($\bar{p}^*$) includes the isotropic part of the turbulent stress tensor. Finally, the source vector is defined as:

$$f \equiv -\left[P_{M1}, \ P_{M2}, \ P_{M3}, \ 0, \ -P_k + \tilde{\varepsilon} + D, \ -c_{\varepsilon 1}P_k\tilde{\varepsilon}/k + c_{\varepsilon 2}f_{\varepsilon 2}\tilde{\varepsilon}^2/k - E\right]^{\text{T}} \tag{18.4}$$

Concerning the momentum source components P_{Mi}, they account for volume sources originating from square and cubic terms in the assumed constitutive relation of equation (14). The EVM closure coefficients are recalled in Table I.

The loosely explicit coupling between the turbulence scale determining equations is strengthened by means of the following decomposition of the source vector f:

$$-\rho f = -\rho\tilde{f} + F_r(\tilde{\boldsymbol{U}}) \tag{19.1}$$

where

$$\tilde{f} \equiv -\left[P_{M1}, \quad P_{M2}, \quad P_{M3}, \quad 0, \quad -P_k + D, \quad -c_{\varepsilon 1} P_k \tilde{\varepsilon}/k - E\right]^{\mathrm{T}}$$
$$F_r(\tilde{\boldsymbol{U}}) = \left[0, \quad 0, \quad 0, \quad 0, \quad c_k k, \quad c_\varepsilon \tilde{\varepsilon}\right]^{\mathrm{T}} \tag{19.2}$$

with,

$$c_k = \frac{\tilde{\varepsilon}}{k} \quad c_\varepsilon = c_{\varepsilon 2} f_{\varepsilon 2} \frac{\tilde{\varepsilon}}{k} \tag{19.3}$$

By that way the dissipation-destruction budget components in $F_r(\tilde{\boldsymbol{U}})$ could be interpreted as reactive terms which are able to establish a direct non-linear coupling. The problem statement (16) could now be rewritten in an advective-diffusive-reactive fashion:

$$\begin{aligned} &F_a(\tilde{\boldsymbol{U}})_{,j} + F_d(\tilde{\boldsymbol{U}}, \nabla\tilde{\boldsymbol{U}})_{,j} + F_r(\tilde{\boldsymbol{U}}) - \rho\tilde{f} = 0 \ \text{ in } \ \Omega \in \mathbb{R}^{\mathrm{nsd}} \\ &\overline{\boldsymbol{U}} = \overline{\boldsymbol{U}}_{\mathrm{D}} \ \text{ on } \ \Gamma_D \\ &F_{d,n} = \theta_{\mathrm{N}} \ \text{ on } \ \Gamma_{\mathrm{N}} \end{aligned} \tag{20}$$

It is thus possible to calculate the reaction numbers for the k-ε equations, that read as:

$$r_k = \frac{c_k h^2}{\nu + \frac{\nu_t}{\sigma_k}} \tag{21.1}$$

$$r_\varepsilon = \frac{c_\varepsilon h^2}{\nu + \frac{\nu_t}{\sigma_\varepsilon}} \tag{21.2}$$

It is remarkable that the magnitudes of the reaction-to-advection ratios (r_k/Pe_k, $r_\varepsilon/Pe_\varepsilon$) become relevant in the near-wall region, mainly within the viscous and buffer sub-layers. Moreover, reaction-driven effects are emphasized in presence of non-equilibrium phenomena such as stagnation region, transition or separation. To this end, it is possible to express the relative magnitude of reaction with respect to advection in terms of time scale ratio:

$$\frac{r_k}{Pe_k} \sim \frac{r_\varepsilon}{Pe_\varepsilon} \sim \frac{\varepsilon}{k}\frac{h}{\|\bar{u}\|} \sim \frac{T}{\tau} \tag{22}$$

Table I.
EVM CLS96 coefficients

σ_k	1
σ_ε	1.3
$C_{\varepsilon 1}$	1.44
$c_{\varepsilon 2}$	1.92
$f_{\varepsilon 2}$	$\left[1 - 0.3\exp\left(-\mathrm{Re}_t^2\right)\right]$
P_k	$u_i' u_k' \bar{u}_{i,k}$
D	$2\nu(\partial\sqrt{k}/\partial x_i)^2$
E	$0.0022 Sk\tau\nu_t(\partial^2\bar{u}_i/\partial x_j\partial x_k)^2$
τ	k/ε

where $T = h/\|\bar{u}\|$ is the element mean time scale and $\tau = k/\varepsilon$ is the modelled turbulence time scale. For instance, in case of a fully developed plane channel flow it is easy to show that approaching the wall T/τ behaves as:

$$\frac{T}{\tau} \sim \frac{1}{\delta^2} \tag{23}$$

where δ is the distance from the solid wall.

SPG variational formulation for RANS equations

Let us define, by using the notation introduced in equations (3.1) and (3.2), the finite dimensional spaces of trial and test functions for primary and constrained variables as:

$$\begin{aligned} S_p^h &= \{\overline{U}_p | \overline{U}_p \in H^{1h}(\Omega),\ \ \overline{U}_p = \varphi_D \ \text{ on } \ \Gamma_D,\ \ \varphi_D \in H^{(1/2)h}(\Gamma_D)\} \\ V_p^h &= \left\{ w_p | w_p \in H_0^{1h}(\Omega),\ \ w_p = 0 \ \text{ on } \ \Gamma_D \right\} \\ S_c^h &= V_c^h = \left\{ \overline{U}_c | \overline{U}_c \in H_0^{1h}(\Omega),\ \ w_c | w_c \in H_0^{1h}(\Omega) \right\} \end{aligned} \tag{24}$$

The associated SPG weight functions could be written in vector form as:

$$\tilde{w} \equiv w + \pi$$

$$w = [\, w_p,\ \ w_p,\ \ w_p,\ \ w_c,\ \ w_p,\ \ w_p \,]^{\mathrm{T}}, \quad \pi = [\, \pi_p,\ \ \pi_p,\ \ \pi_p,\ \ \pi_c,\ \ \pi_p,\ \ \pi_p \,]^{\mathrm{T}}, \tag{25}$$

where the Galerkin test functions are modified by the perturbation π. The perturbation for the primary-turbulent variables π_p is based on the operator already introduced in equation (10) for the scalar problem. In addition PSPG stabilization is used, also for mixed order Q2-Q1 elements, making the convergence faster by means of zero diagonal entries elimination (Borello *et al.*, 2003). The resulting perturbation of the continuity equation, which is made proportional to the momentum residual, makes use of a function π_c that reads as:

$$\pi_c = \frac{h}{2\|U\|} \zeta w_{c,j} \tag{26}$$

where U is the global scaling velocity, and the dependence on the element Peclet number is exploited through the ζ magic function proposed by Tezduyar *et al.* (1992).

The residual SPG formulation of the differential problem (18.1)-(18.4) now reads as follows: find $\overline{U} \in H^{1h}\ \forall w_p \in V_p^h, \forall w_c \in V_c^h$, such that:

$$c(\bar{u}, \overline{U}, w) + s(\overline{U}, w) + r(\overline{U}, w) + \Pi(\pi) = (\rho \tilde{f}, w^h) + (\varphi_N, w_{\Gamma_N})_{\Gamma_N} \tag{27}$$

with use of bi-linear and tri-linear forms:

$$
\begin{aligned}
s(\overline{U}, w) &= -\int_{\Omega} w_j F_d \, \mathrm{d}\Omega \\
(\rho\tilde{f}, w) &= \int_{\Omega} w\rho\tilde{f} \, \mathrm{d}\Omega \\
(\varphi_N, w_{|\Gamma_N})_{\Gamma_N} &= \int_{\Gamma} w_{\Gamma_N} \varphi_N \, \mathrm{d}\Gamma \\
c(\bar{u}; \overline{U}, w) &= \int_{\Omega} F_{a,j} w \, \mathrm{d}\Omega \\
r(\overline{U}, w) &= \int_{\Omega} w F_r \, \mathrm{d}\Omega
\end{aligned}
\tag{28}
$$

Finally, the stabilization integrals are defined as:

$$
\begin{aligned}
\Pi(\pi_p) &= \sum_{e=1}^{\mathrm{nel}} \int_{\Omega_e} (F_{a,j} + F_{d,j} + F_r - \rho\tilde{f}) \pi_p \, \mathrm{d}\Omega \\
\Pi(\pi_c) &= \sum_{e=1}^{\mathrm{nel}} \int_{\Omega_e} (F_{a,j} + F_{d,j} + F_r - \rho\tilde{f})^{(M)} \pi_c \, \mathrm{d}\Omega
\end{aligned}
\tag{29}
$$

where the superscript $^{(M)}$ refers to the momentum residual, and the stabilizing contributions are confined on the element interior according to the continuity properties of the lower order perturbation function.

Numerical examples

In this section, we assess the numerical performance of the proposed SPG formulation for model problems as well as flow configurations pertinent to turbomachinery fluid dynamics. In these validation studies, the improvement of the SPG are commented with respect to the classical stabilization schemes, such as the SUPG or streamline upwind. It is remarkable that, since all of the consistent methods usually share the optimal property in 1D, the proposed test cases violate at least one of the super-convergence conditions (i.e. non-uniform mesh, multi-dimensional domain, non-linear equations and non-homogeneous source terms).

Advection-diffusion-reaction 2D model problem

The first test cases (labelled TC1 and TC2) concern the numerical solution of the linear scalar advective-diffusive-reactive model problem (1.1) and (1.2), in a unit square domain. The mesh is uniform with 10×10 quadratic elements, thus consisting of 441 nodes. The complete problem statements are shown in Figure 4, for both TC1 and TC2. The known velocity field u is assumed to have a parabolic profile (e.g. $u(x,y) = 2y - y^2$, $v(x,y) = 0$), with maximum value equal to one. The coefficients are: $k = 10^{-5}$, $c = 5 \times 10^2$, and the related maxima for dimensionless numbers are: $Pe = o(10^3)$ and $r = o(10^5)$, obtained with a pure geometrical element characteristic length h.

For both test cases the SPG solutions are compared to quadratic Galerkin (G Q2), streamline upwind (SU Q2) and SUPG Q2 ones. First, in Figure 5 numerical solutions for TC1 are compared. As it clearly appears, the SU Q2 is unable to the improve Galerkin solution, suffering from the combination of its inconsistency and its inability

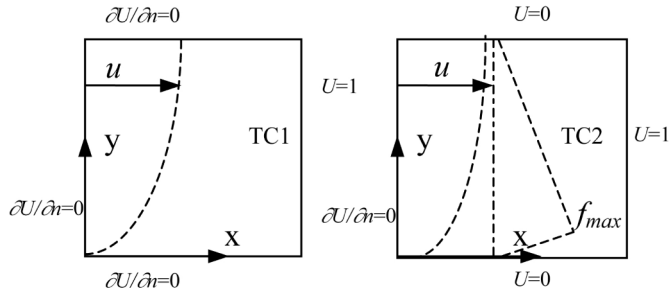

Figure 4.
Scalar advective-diffusive-reactive problem statement: TC1, $f = 0$; TC2, $f_{\max}(y = 0.1) = 50$

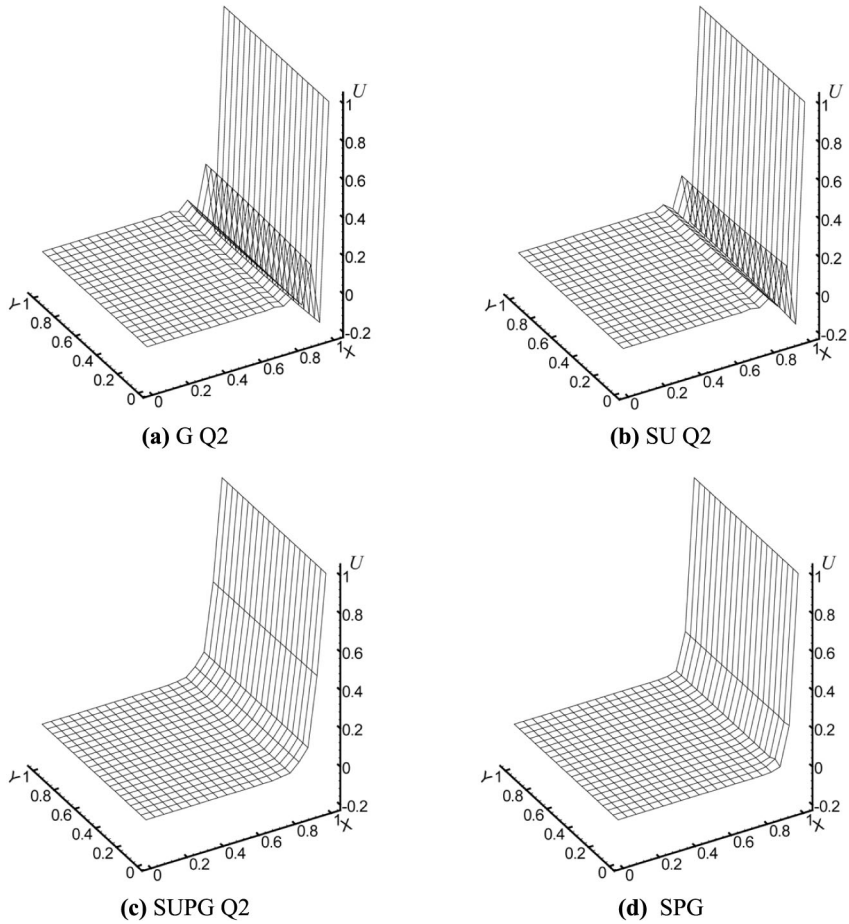

(a) G Q2 **(b)** SU Q2 **(c)** SUPG Q2 **(d)** SPG

Figure 5.
TC1 comparison of solution

to control reactive effects. With respect to the PG schemes, both feature stable fields, being able of controlling completely the instability origins in the near- and far-wall regions.

Figure 6 shows the U streamwise profiles predicted by G Q2, SUPG Q2 and SPG schemes at $y = 0.05$ and $y = 0.1$, close to the null advection boundary line, with a list of the last nodal values. The PG-like solutions are both able of predicting smooth U profiles, improving the G Q2 and SU Q2 oscillatory behaviour. Nonetheless, the SUPG Q2 returns an over-diffused layer close to the Dirichlet conditions, thus confirming its inability to control the reactive effects, with respect to SPG solution that returns a sharp but continuous solution layer.

As far as the TC2 case with non-uniform source f is concerned, in Figure 7 the solutions are compared.

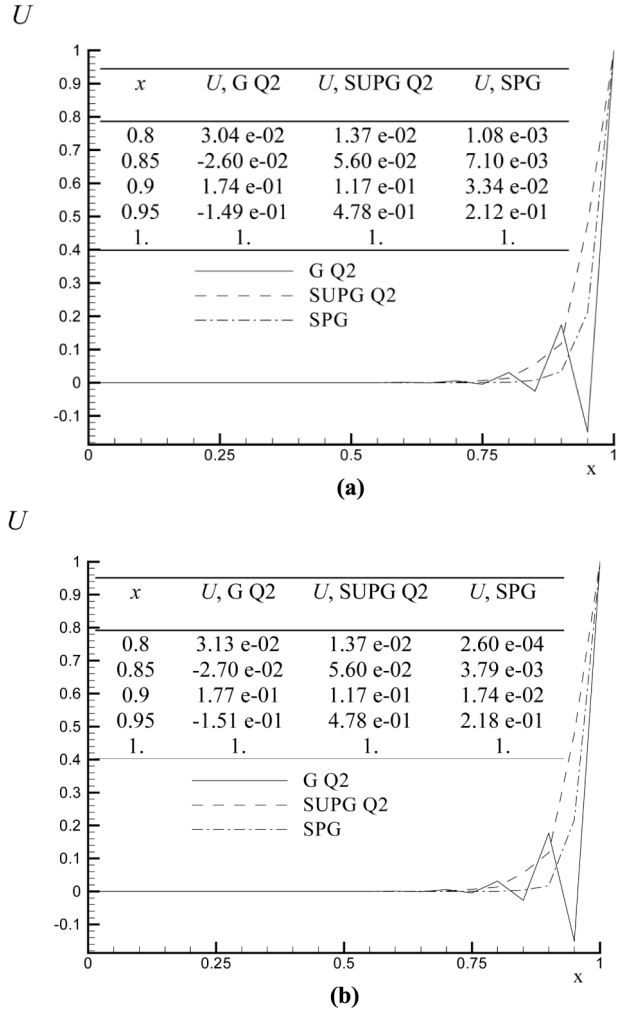

Figure 6.
TC1 comparison of streamwise U profiles: (a) at $y = 0.05$; and (b) at $y = 0.1$

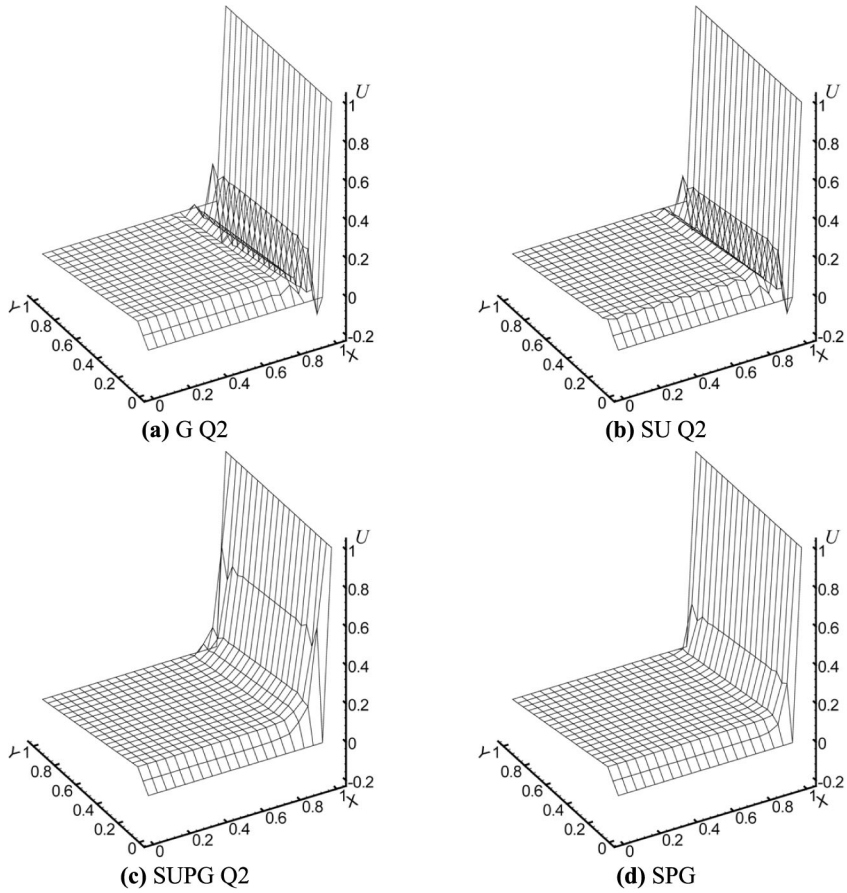

(a) G Q2 **(b)** SU Q2

(c) SUPG Q2 **(d)** SPG

Figure 7.
TC2 comparison

It is worth noting that the source integral has been approximated linearly, according to the Q2 element optimal conditions (Codina *et al.*, 1992). Even in this case the SU Q2 solution suffers from the same oscillations arising in the Galerkin one. In Figure 8 are compared the U streamwise profiles predicted by G Q2, SUPG Q2 and SPG schemes at $y = 0.05$ and $y = 0.1$. In this flow region the reactive effects are combined with a steep gradient of the source term.

The comparison between the shown nodal values confirms that the SPG is able to recover a non-oscillatory solution, also where the sharp streamwise solution layer develops under the effect of a non-uniform source. In addition to the higher diffusivity of the SUPG solution, Figure 7(c) shows some numerical pathologies due to the presence of the relevant source term.

Turbulent flow on a semi-circular leading edge

The second test case concerns the prediction of the boundary layer development on a flat plate with a semi-circular leading edge. The leading-edge configuration, labelled T3L, was proposed in 1991 by the ERCOFTAC Special Interest Group on Transition. In

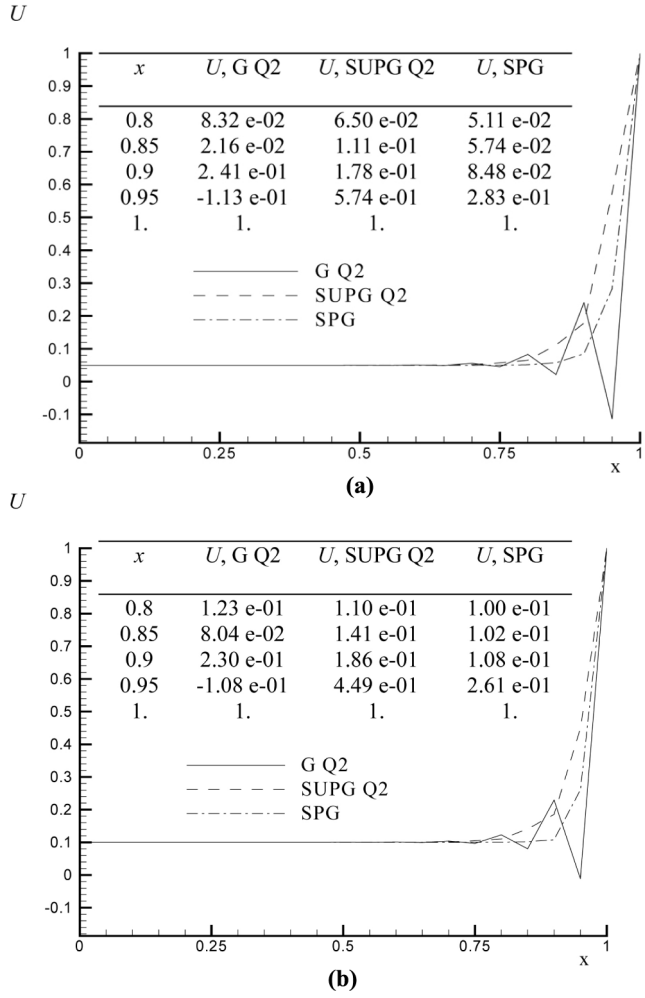

Figure 8.
TC2 comparison of streamwise U profiles: (a) at $y = 0.05$; and (b) at $y = 0.1$

particular, the present study refers to the experiments carried out by Palikaras *et al.* (2002) for the zero pressure gradient configuration. The Reynolds number, based on the inlet velocity and the leading-edge radius ($l_r = 5\,\text{mm}$), is equal to 1,660. The flow is assumed 2D with constant temperature and incompressible, with an experimental inlet free-stream turbulence intensity (TI) set to 7 per cent, and a dissipation length l_ε of 18 mm.

The computational domain, that extends 15 l_r upstream the leading edge and 60 l_r downstream of it, has been modelled with a 12,681 nodes block-structured (H-O) grid, and Q2-Q1 element pair. In the vicinity of the flat plate (i.e. O-connected region) the first node row has a dimensionless distance from the solid wall $\delta^+ = y^+ = 1.0$. On the inlet section of the computational domain, the experimental free-stream uniform profile is used for the velocity ($\bar{u} = 5\,\text{m/s}$), and uniform distributions are also used for the

turbulent unknowns (i.e. k and $\tilde{\varepsilon}$) which are computed on the basis of the measured TI and l_ε. No-slip conditions are used on the plate wall, and homogeneous Neumann conditions are imposed on the outlet section.

The numerical campaigns for the SPG scheme assessment were carried out using the FGMRES(20) solver with convergence thresholds for error R_{res} and solution R_{sol} residuals set to 10^{-6}. Uniform initial fields were used for velocity components and turbulent variables, setting $\bar{u}$, k and $\tilde{\varepsilon}$, respectively, to the free-stream values and $\bar{v} = \bar{u}$ 0.01. The stabilization parameters have been computed by means of the streamwise characteristic element length (Tezduyar *et al.*, 1992), and a quadratic SUPG formulation (Codina *et al.*, 1992) was used to produce the benchmark solution.

The first analysis takes into account the numerical robustness by comparing, in Figure 9, the convergence histories in terms of the R_{sol} and R_{res}.

The plotted data refer to the use of SPG and SUPG stabilized formulations on RANS equations with a standard eddy viscosity closure, e.g. the k-ε model proposed by Launder and Sharma (1974). The shown R_{sol} and R_{res} behaviours provide the evidence that the SPG produces a slight speed-up into the convergence.

The analysis of the SPG formulation when applied to the solution of the flow and turbulence equations in a fully coupled manner, was then extended to a RANS closure based on an anisotropic turbulence model, e.g. the cubic k-ε model CLS96. That is considered as a fair baseline in turbomachinery simulation, as it includes provisions to account for curvature and non-equilibrium effects, and to attenuate stagnation-point inconsistency (Corsini and Rispoli, 2002). The assessment of the SPG features in presence of turbulence-related reactive effects was focused on the T3L flow regions typically affected by non-equilibrium phenomena. In order to figure out the magnitude of the resolved advective-reactive values, Figure 10 shows the contours of the ratio r_k/Pe_k about the leading-edge profile in the case of the SPG

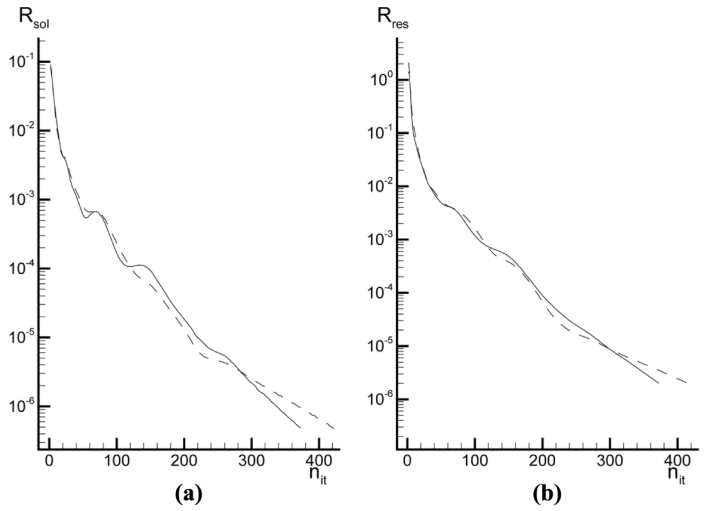

Note: Solid line: SPG; dashed line: SUPG

Figure 9.
T3L convergence histories for PG formulations: (a) R_{sol}; and (b) R_{res}

solution. The isolines show that the reactivity of the turbulence equations manifests itself in the vicinity of the stagnation point, and downstream the leading edge starting from the axial location where the onset of the by-pass laminar-to-turbulence transition falls. It is worth noting that within the reactivity cores the reaction number r_k has a magnitude comparable to that of the local advection, while moving downstream its value grows up to $o(10^3)$.

Moving downstream the leading edge, the assessment of the SPG formulation against the SUPG one deals with the simulation of the boundary layer development in terms of streamwise-velocity profiles and integral boundary layer parameterisation (Figure 11).

In Figure 12, the streamwise-velocity evolution along the flat plate shows no remarkable differences between the computed profiles, both in fair agreement with the experimental data. Instead, Figure 12 compares the axial evolution of the integral properties of the flat plate boundary layer. The following quantities have been plotted against the available measurements: the displacement δ^* and momentum θ^* thicknesses, and the shape factor H.

Contrarily to the velocity profiles, the axial evolutions of the displacement thickness, in Figure 12(a), provide the evidence of differences between the PG formulations under exam. Though the computational data under-predict the measured one, the SPG δ^* distribution shows an improved capability of mimicking the velocity layer thickness evolution up to a fully-turbulent state, featuring higher δ^* values and similar axial profile shape. This circumstance is further confirmed by the momentum thickness distributions, Figure 12(b). Here the SPG is shown to return qualitatively the variation of the boundary layer momentum content reproducing also the profile gradient discontinuity at the transition onset (e.g. $x = 0.008$, $x/l_r = 1.6$). Figure 12(c), finally, compares the shape factor evolutions. It is remarkable that, though under-predicting the experiments, the SPG solution is able of recovering a profile shape similar to the measured one and mainly characterized by the abrupt slope variation in the transition region where, as shown in Figure 10, r and Pe assume a comparable magnitude.

Figure 13, moreover, investigates the streamwise evolution of the boundary layer in terms of the TI profile normal to the wall.

The TI field, explicitly affected by the reactivity of the implemented turbulence equations, shows that the SPG solution outperforms the SUPG one in predicting the

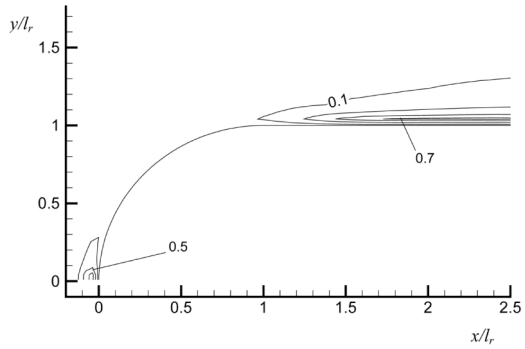

Figure 10.
Reaction-to-advection ratio r_k/Pe_k contours

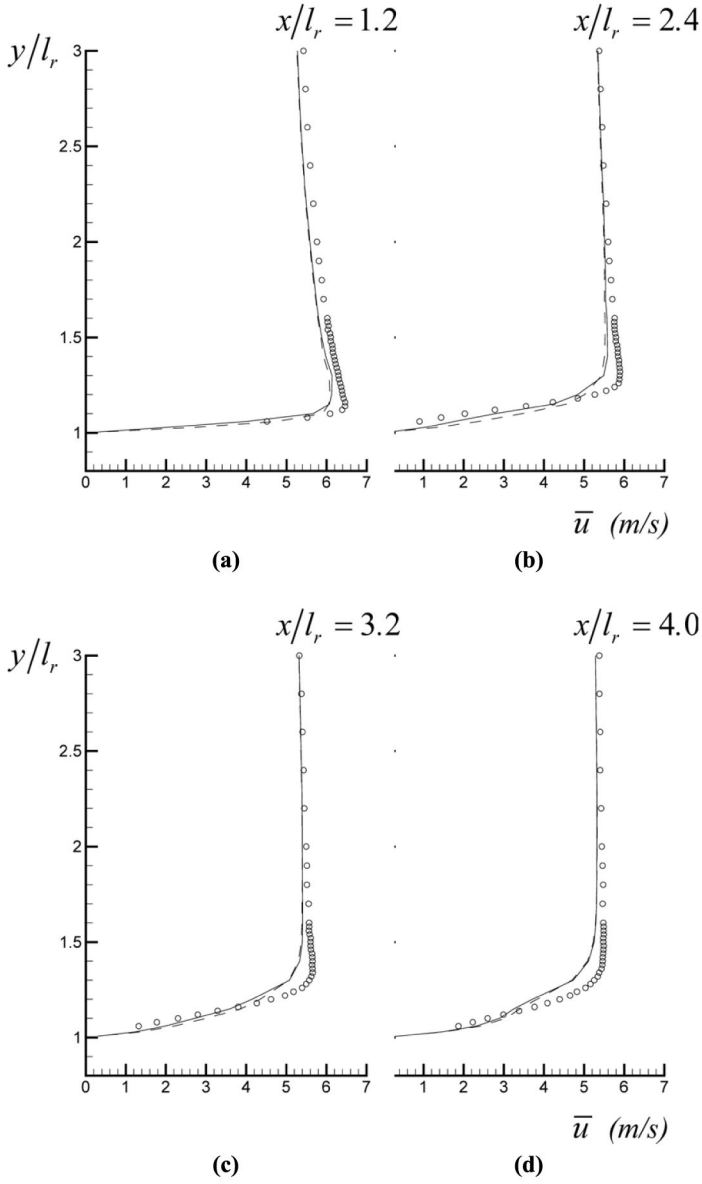

Note: Symbols: experiments; dashed line: SUPG; solid line: SPG

Figure 11.
Streamwise velocity profiles

re-arrangement of the boundary layer. In detail, the u' profiles at $x/l_r = 1.2$ clearly show that in the buffer-layer region, where the local reaction number is of $o(10^0)$, the SPG is able of reducing the over-prediction of the local turbulence level related to the well known EVM failure of correctly detecting the by-pass transition.

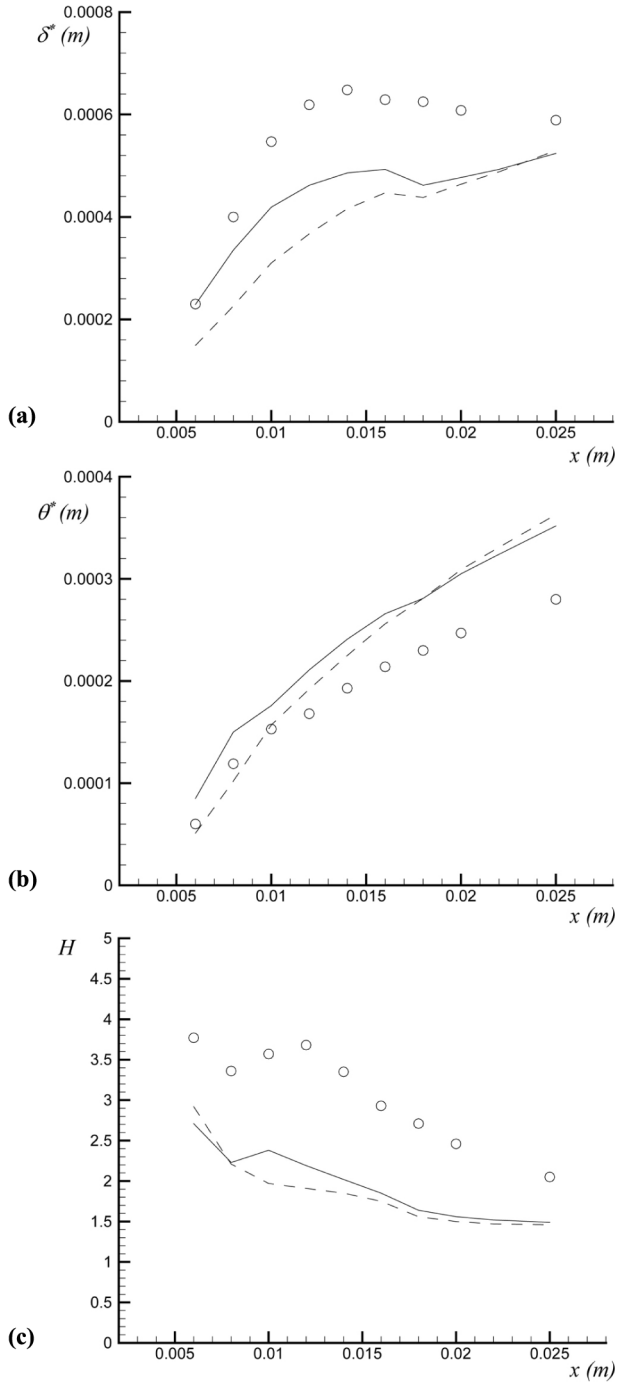

Figure 12.
Integral boundary layer parameters:
(a) displacement thickness;
(b) momentum thickness;
and (c) shape factor

Note: Symbols: experiments; dashed line: SUPG; solid line: SPG

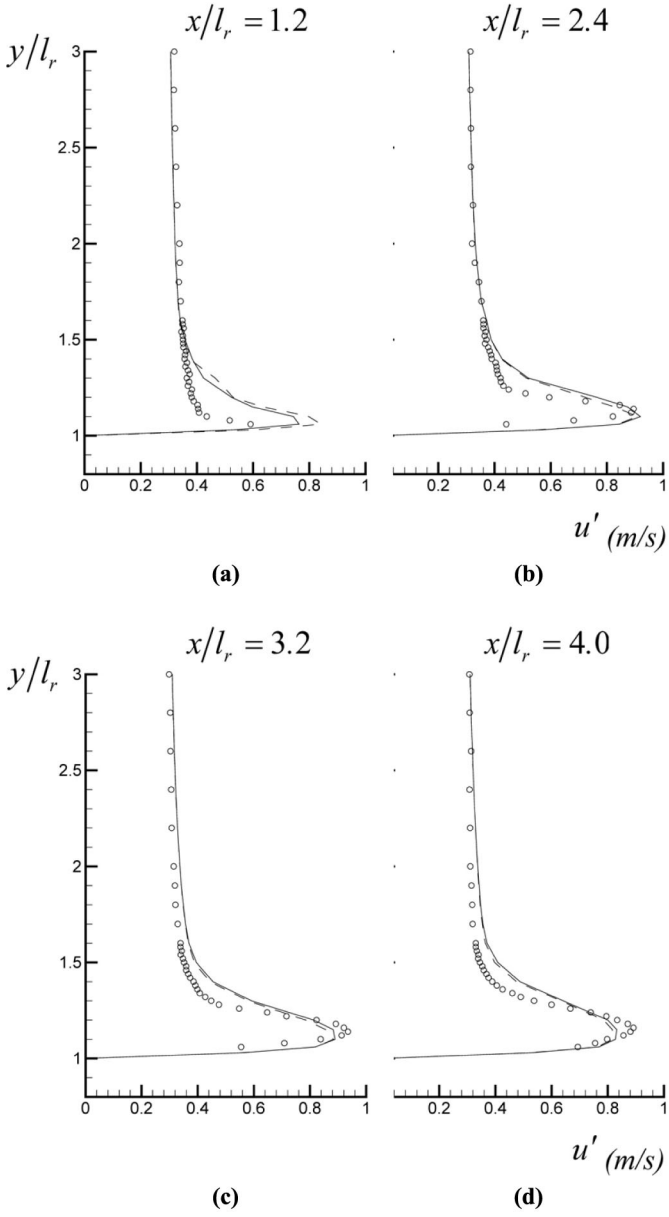

Note: Symbols: experiments; dashed line: SUPG; solid line: SPG

Figure 13.
Streamwise TI profiles

Controlled-diffusion compressor cascade flow

The last test case concerns a 2D compressor cascade with controlled-diffusion (CD) blade profile, designed by Sanger (1983) and experimentally studied by Elazar and Shreeve (1990) using two-component LDV system. The blade profile has a

14.4° stagger angle, a solidity $\sigma = 1.67$, and a chord length $l_c = 127.3$ mm. Three inlet flow angles were measured (quasi-design, weak off-design, off-design) and only the off-design condition with incidence angle β equal to 46° is here considered. In this condition, the suction side is subjected to a strong adverse pressure gradient, that promotes a challenging transitional flow, with a boundary layer becoming thicker and thicker as the trailing edge is approached (Chen *et al.*, 1998). The chord Reynolds number, based on the inlet flow velocity U_{in} (= 85 m/s), is set to 7×10^5. The flow is 2D with constant temperature, and could be considered virtually incompressible. A H topology consisting of 40,524 nodes was used to model the flow region, as sketched in Figure 14. The refinement is such that the highest dimensionless distance for the nearest node to the wall along the boundary is $\delta^+ = 1.5$. The numerical campaigns for the SPG scheme assessment were carried out using the FGMRES(20) solver with convergence thresholds for error R_{res} and solution R_{sol} residuals set to 10^{-6}.

At the inlet section of the computational domain uniform profiles are used for the velocity components and the turbulent quantities. The experimental free-stream distribution is used for the mean velocity profile. The TI and the characteristic length scale are TI = 2.3 and $l_\varepsilon/l_c = 3$ per cent. These return the physical turbulence level at the blade leading edge, located half a chord downstream the inlet plane. Homogeneous Neumann conditions are used at the outlet section, one chord downstream the trailing edge, and the flow periodicity is strictly imposed at the permeable boundaries in the middle of adjacent blade passages.

Figure 15 shows the contours of the ratio r_k/Pe_k in the vicinity of the blade leading and trailing edges for the SPG solution. As a consequence of the chosen operating condition, with the flow entering the blade row at the maximum incidence, the isolines indicate the presence of high reactivity cores approaching the stagnation point and along the blade suction side with a peak value of $o(10^1)$.

The experimental static pressure coefficient C_p distribution, shown in Figure 16, suggests the existence of a substantial uniform adverse pressure gradient governing the boundary layer evolution on the suction downwind the leading edge. The PG formulations appear to be, quite generally, in fairly sensitive matching with the measured pressure distribution, and both approximate the pressure profile flattening about 15 per cent of the chord that traces the leading-edge separation.

The streamwise-velocity and TI distributions on the blade suction side are plotted, respectively, in Figures 17 and 18 at three chordwise locations: $x/l_c = 5.2$, 64 and 95 per cent against the non-dimensional distance δ/l_c.

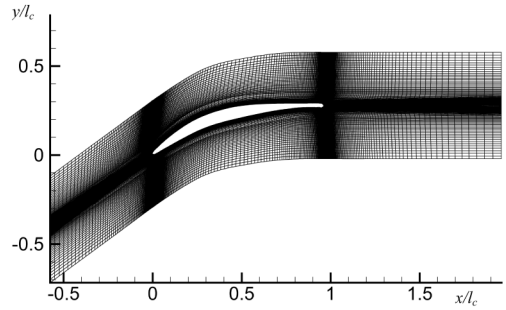

Figure 14.
Controlled diffusion cascade, computational grid

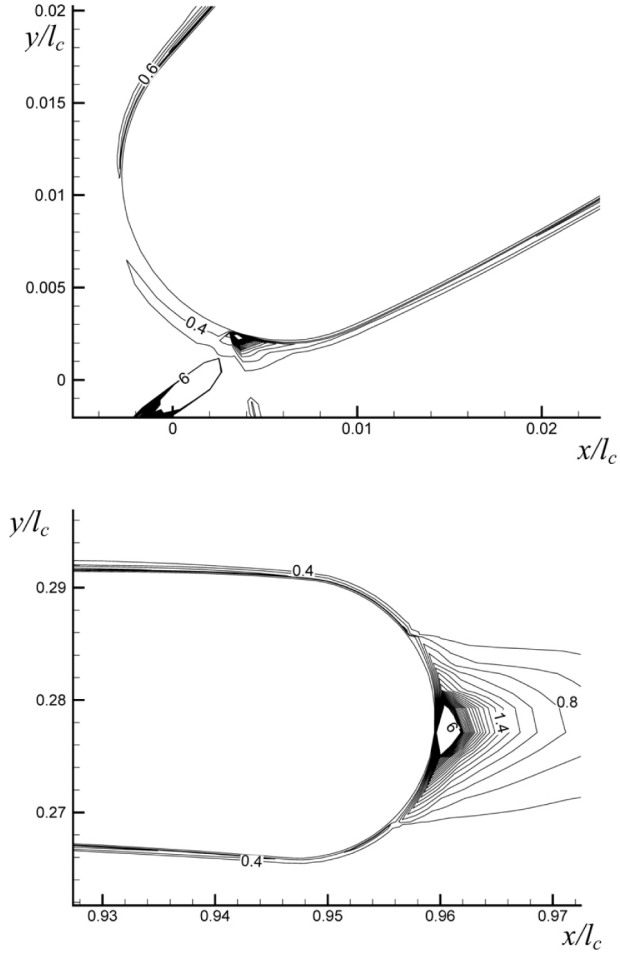

Figure 15.
Reaction-to-advection ratio r_k/Pe_k contours

Both the computed boundary layer developments appear to return the physical issues shown by the experiments, within the inner and the outer layers. It is important to note that the presence of an adverse pressure gradient, causing the reactivity to be more relevant compared to the T3L configuration, gives rise to noticeable differences in the streamwise-velocity and TI profiles. In detail, the SPG appears to resolve the boundary layer thickening and the turbulence energy contents in a far better agreement than the SUPG scheme.

Influence of the SPG formulation on turbulence phenomena prediction

The flat plate and compressor cascade studies discussed above, have provided evidence that the application of the SPG residual scheme to the RANS equations with an anisotropic eddy viscosity closure had enabled the turbulence phemonena to be realistically captured in flow configuration pertinent to turbomachinery. Moreover, the proposed advective-diffusive-reactive PG formulation improves the solution accuracy

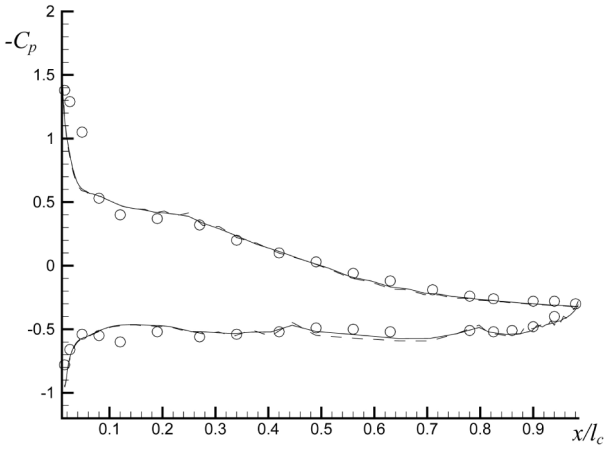

Figure 16.
C_p distributions

Note: Symbols: experiments; dashed line: SUPG; solid line: SPG

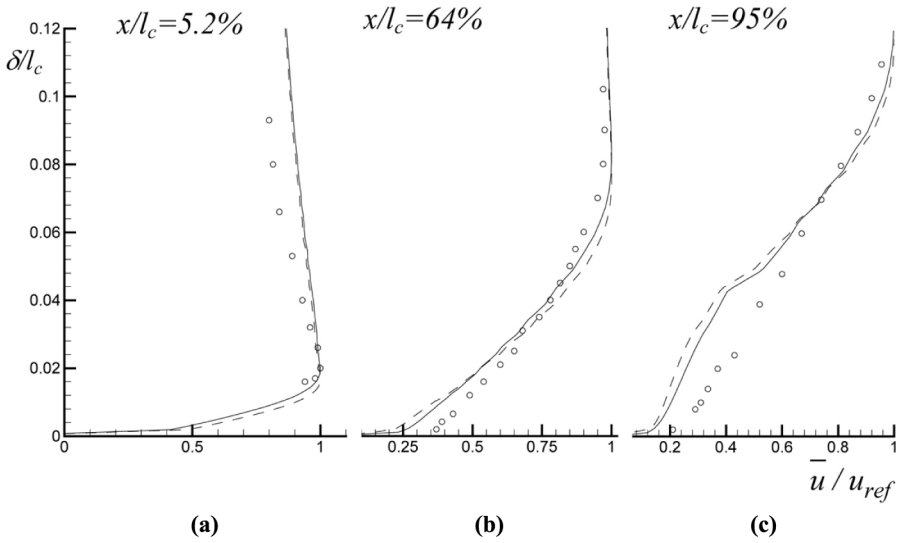

Figure 17.
Streamwise velocity profiles

Note: Symbols: experiments; dashed line: SUPG; solid line: SPG

with respect to a standard streamline driven stabilization schemes, e.g. the SUPG, in that it properly accounts for the boundary layer region flow phenomena in presence of non-equilibrium effects. With the aim of contributing to understand the influence of the SPG residual scheme we focus on those issues shown by the simulation of boundary layer in presence of zero and strong adverse pressure gradient, and in the leading-edge stagnation region.

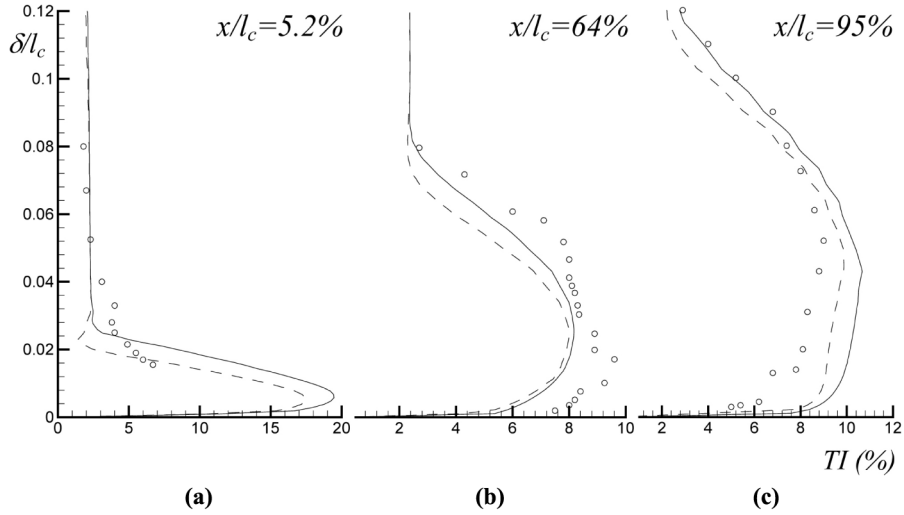

Note: Symbols: experiments; dashed line: SUPG; solid line: SPG

Figure 18.
Streamwise TI profiles

As far as the boundary layer simulations are concerned, the SPG solution outperforms the purely advective scheme resolving adequately the axial and chord-wise evolution of the velocity layer thickness (Figures 11 and 17) as well as the turbulent energy contents (Figures 13 and 18). In this respect the insufficient cross-wise turbulent mixing shown by the SUPG solutions, that typically affects the non-linear EVM owing to the cubic stress-strain relationship (Chen *et al.*, 1998; Corsini and Rispoli, 2002), appears to be attenuated. This feature origins from the dependence of the residual distributor mechanism from the reaction magnitude, through the numbers r_k and r_ε. The weight additive structure proposed in equation (10) is able to correct, on an element scale, the spatial shape of the projection operator balancing the purely anisotropic streamwise deformation with an elliptic diffusive-reactive effect.

To demonstrate this concept, with reference to the T3L configuration, Figure 19 shows the profiles normal to the wall of the turbulent viscosity ν_t (Figure 13(c)) at two axial locations, $x/l_r = 1.2$ and 2.4.

Figure 19 clearly shows that the SPG affects the cross-wise ν_t distribution by reducing it within the low reactivity core before the transition completion (Figure 19(a)), and by increasing it downstream where the reactivity grows (Figure 19(b)), producing an enhanced turbulence transport by diffusive dominated mechanisms. Furthermore, Figure 20 shows the crosswise profiles of the turbulent diffusive component $D_t = \nu_t \partial^2 k/\partial y^2$ of the k equation budget at $x/l_r = 1.2$ and 2.4. Data in Figure 20 are normalized with respect to the local friction velocity u_τ and the molecular viscosity ν.

The analysis of D_t behaviours gives an additional *a-posteriori* confirmation of the SPG ability to adapt the shape of the residual projector resolving adequately the crosswise diffusion enhancement correlated to the boundary layer transition to the fully turbulent state (e.g. about $y+ = 25$ the D_t enhances according to a ratio 1:8 in the SPG simulation).

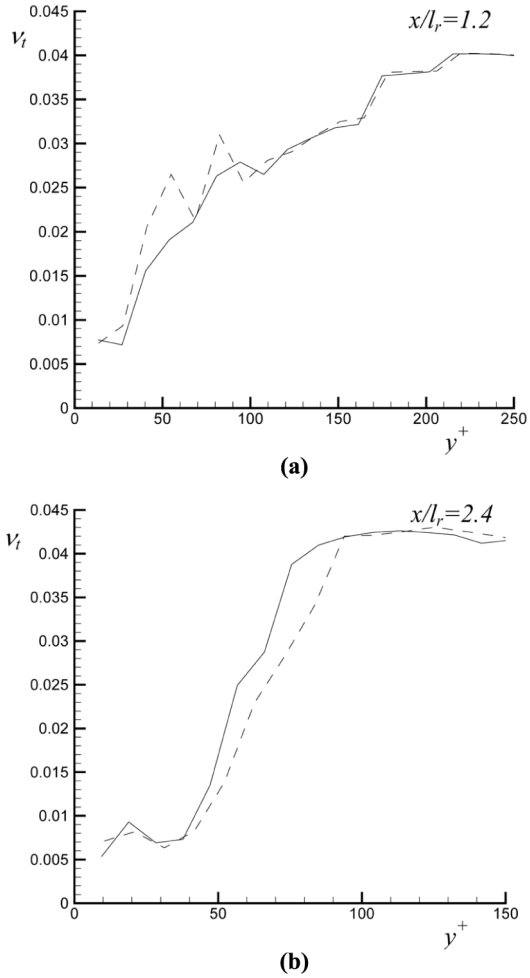

Figure 19.
T3L, non-dimensional turbulence viscosity profiles normal to the wall, ν_t (m^2/s)

Note: Dashed line: SUPG; solid line: SPG

Finally, to give more hints about the influence of the SPG scheme in the vicinity of the stagnation point region, the behaviour of the turbulence time scale $t = k/\varepsilon$ is discussed owing to its influence on the production of ε that is recognized to cause spuriously high turbulent kinetic energy level (Durbin, 1996). Figure 21 compares the profiles of the computed turbulence time scale $\tau(x)$ along a stagnation line from the axial position $x/l_r = -0.3$. As shown in Figure 21, independently from the PG formulation, the use of an anisotropic EVM is able to control the over-prediction of τ eliminating the anomalously large turbulent kinetic energy growth (e.g. so-called stagnation point anomaly) without introducing scale-limiter in the form of realizability constraint (Corsini and Rispoli, 2002). It is, moreover, evident that the SPG profile features a further abatement of τ with a

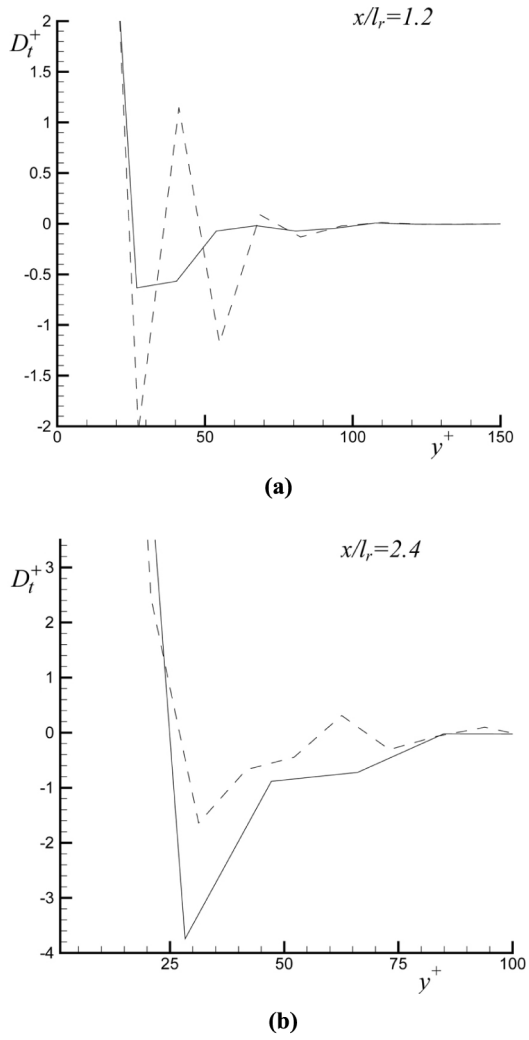

Note: Dashed line: SUPG; solid line: SPG

Figure 20.
T3L k budget, normalized turbulent diffusion contribution normal to the wall

ratio 2:3 in the peak value, as already shown by Corsini *et al.* (2003) for a standard EVM. On the basis of equation (27), the remarked improvement in the time-scale limit is related to the sensitivity that the SPG residual projection basis from the evolution of τ, as indicated by c_k and c_ε in equation (19.3), that becomes critical approaching a pure reactive-diffusive flow limit.

Conclusions

This paper investigated the predicting capabilities of a FEM stabilized formulation developed for the purpose of solving advection-reaction-diffusion problems. Such a

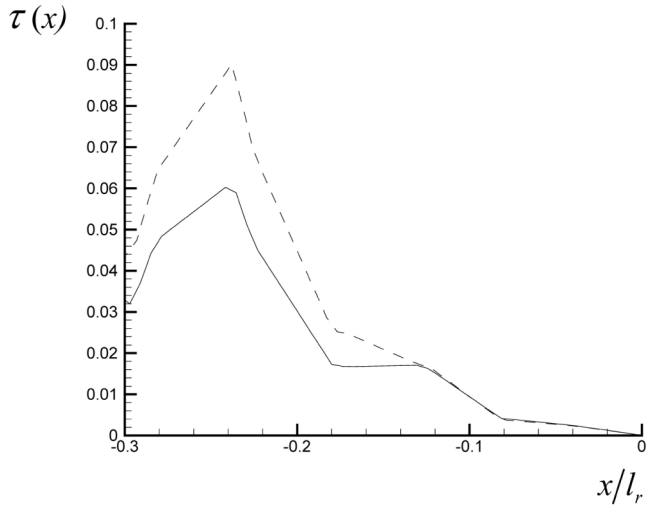

Figure 21.
Turbulence time scale behaviour approaching the stagnation point

Note: Solid line: SPG; dashed line: SUPG

scheme, called SPG, addresses the use of a perturbation to the weight function composed by two contributions on quadratic finite elements. The first one is a SUPG like operator and is used to overcome wiggles due to advective or skew-symmetric terms, whereas the second one is a symmetric operator aiming at precluding oscillations due to reactive terms. The FEM formulation has been obtained by means of 1D nodal exactness, but has been tested in several more complex examples that violate the super convergence conditions. In this respect, the SPG method demonstrates its suitability in solving the typical equations of turbulence eddy viscosity models.

References

Borello, D., Corsini, A. and Rispoli, F. (2003), "A finite element overlapping scheme for turbomachinery flows on parallel platforms", *Computers & Fluids*, Vol. 32, pp. 1017-47.

Brezzi, F., Marini, D. and Russo, A. (1998), "Applications of the pseudo residual-free bubbles to the stabilization of convection-diffusion problems", *Computer Methods in Applied Mechanics and Engineering*, Vol. 166, pp. 51-63.

Chen, W.L. and Leschziner, M.A. (1999), "Modelling turbomachine-blade flows with non-linear eddy-viscosity models and second moment closure", IMechE Paper C557/131/99, A, pp. 189-99.

Chen, W.L., Lien, F.S. and Leschziner, M.A. (1998), "Computational prediction of flow around highly loaded compressor cascade blades with non-linear eddy-viscosity models", *International Journal of Heat and Fluid Flow*, Vol. 19, pp. 307-19.

Codina, R. (2001), "A stabilized finite element method for generalized stationary incompressible flows", *Computer Methods in Applied Mechanics and Engineering*, Vol. 190, pp. 2681-706.

Codina, R. and Soto, O. (1997), "Finite element solution of the Stokes problem with dominating Coriolis force", *Computer Methods in Applied Mechanics and Engineering*, Vol. 142, pp. 215-34.

Codina, R., Oñate, E. and Cervera, M. (1992), "The intrinsic time for the streamline upwind/Petrov-Galerkin formulation using quadratic elements", *Computer Methods in Applied Mechanics and Engineering*, Vol. 94, pp. 239-62.

Corsini, A. and Rispoli, F. (2002), "Anisotropic turbulence modeling of near wall effects pertinent to turbomachinery flows", ASME Paper FEDSM02-31206.

Corsini, A., Rispoli, F. and Santoriello, A. (2003), "A new stabilized finite element method for advection-diffusion-reaction equations using quadratic elements", *CMFF '03 Proceedings*, II, pp. 791-9.

Craft, T.J., Launder, B.E. and Suga, K. (1996), "Development and application of a cubic eddy-viscosity model of turbulence", *International Journal of Heat and Fluid Flow*, Vol. 17, pp. 108-55.

Durbin, P.A. (1996), "On the k-ε stagnation point anomaly", *International Journal of Heat and Fluid Flow*, Vol. 17, pp. 89-90.

Elazar, Y. and Shreeve, R.P. (1990), "Viscous flow in a controlled diffusion compressor cascade with increasing incidence", *Transactions of the ASME*, Vol. 112, pp. 256-66.

Harari, I. and Hughes, T.J.R. (1994), "Stabilized finite element methods for steady advection-diffusion with production", *Computer Methods in Applied Mechanics and Engineering*, Vol. 115, pp. 165-91.

Hughes, T.J.R. and Brooks, A.N. (1982a), "Streamline upwind/Petrov-Galerkin formulations for convection dominated flows with particular emphasis on the incompressible Navier-Stokes equations", *Computer Methods in Applied Mechanics and Engineering*, Vol. 32, pp. 199-259.

Hughes, T.J.R. and Brooks, A. (1982b), "A theoretical framework for Petrov-Galerkin methods with discontinuous weighting functions: application to the streamline-upwind procedure", *Finite Elements in Fluids*, Vol. 4, pp. 47-65.

Idelsohn, S., Nigro, N., Storti, M. and Buscaglia, G. (1996), "A Petrov-Galerkin formulation for advection-reaction-diffusion problems", *Computer Methods in Applied Mechanics and Engineering*, Vol. 136, pp. 27-46.

Launder, B.E. and Sharma, B.I. (1974), "Application of the energy dissipation model of turbulence to the calculation of flow near a spinning disc", *Letters in Heat and Mass Transfer*, Vol. 2.

Palikaras, A., Yakinthos, K. and Goulas, A. (2002), "Transition on a flat plate with a semi-circular leading edge under uniform and positive shear free-stream flow", *International Journal of Heat and Fluid Flow*, Vol. 23, pp. 455-70.

Sanger, N.L. (1983), "The use of optimisation techniques to design controlled-diffusion compressor blading", *ASME Journal of Engineering for Power*, Vol. 105, pp. 256-64.

Tezduyar, T.E., Mittal, S., Ray, S.E. and Shih, R. (1992), "Incompressible flow computations with stabilized bilinear and linear equal-order-interpolation velocity-pressure elements", *Computer Methods in Applied Mechanics and Engineering*, Vol. 95, pp. 221-42.

Further reading

Brezzi, F., Franca, L.P., Hughes, T.J.R. and Russo, A. (1997), "$b = \int g$", *Computer Methods in Applied Mechanics and Engineering*, Vol. 145, pp. 329-39.

Appendix 1

In order to clarify all the analytical aspects concerning the SPG stabilized formulation (equations (13.1) and (13.2)), the authors include a complete list of all the adopted symbols and coefficients:

$$
\begin{aligned}
a_7 &= \left[-4 - 2Pe + r/10 - 4Pe\zeta_{a_2} + \frac{r}{2}\zeta_{a_2} + \frac{C_{\mathrm{SPG}}}{280}\zeta_{r_2}Pe + \frac{C_{\mathrm{SPG}}}{140}\zeta_{r_2} - \frac{53C_{\mathrm{SPG}}}{26,880}r\zeta_{r_2}\right] \\
d_8 &= \left[8 + r4/5 + 8Pe\zeta_{a_2} - \frac{C_{\mathrm{SPG}}}{70}\zeta_{r_2} - \frac{C_{\mathrm{SPG}}}{840}r\zeta_{r_2}\right] \\
a_6 &= \left[-4 + 2Pe + r/10 - 4Pe\zeta_{a_2} - \frac{r}{2}\zeta_{a_2} - \frac{C_{\mathrm{SPG}}}{280}\zeta_{r_2}Pe + \frac{C_{\mathrm{SPG}}}{140}\zeta_{r_2} - \frac{53C_{\mathrm{SPG}}}{26,880}r\zeta_{r_2}\right]
\end{aligned}
\tag{A1}
$$

$$
\begin{aligned}
a_1 &= -8 - 4Pe + r/5, \quad b_1 = -8Pe + 12 + r, \\
a_2 &= 1 + Pe - r/10, \quad b_2 = Pe - 6 - r/4, \\
a_3 &= -8 + 4Pe + r/5, \quad b_3 = -8Pe - 12 - r, \\
a_4 &= 14 + r4/5, \quad b_4 = 14Pe, \\
a_5 &= 1 - Pe - r/10, \quad b_5 = Pe + 6 + r/4, \\
e_1 &= -C_{\mathrm{SPG}}(1/35 + r/420), \\
e_2 &= -C_{\mathrm{SPG}}(53r/13,440 - Pe/140 - 1/70), \\
e_3 &= -C_{\mathrm{SPG}}(1/35 + r/420), \\
e_4 &= -C_{\mathrm{SPG}}(53r/6,720 - 1/35), \\
e_5 &= -C_{\mathrm{SPG}}(53r/13,440 + Pe/140 - 1/70), \\
C_{\mathrm{SPG}} &= (2^{12}/3^2)0.35.
\end{aligned}
\tag{A2}
$$

Appendix 2

In the following, the authors report on the final expression of the tuning functions introduced with the SPG stabilized formulation. The notation is coherent with that used in equations (13.1), (13.2), (A1) and (A2), and the fulfilment of the super-convergence feature (i.e. identity between numerical solution and exact one for linear homogeneous 1D problems) permits to obtain the following results:

$$
\begin{aligned}
\zeta_{a_2} &= \frac{4}{5}r\frac{\left[\begin{array}{c}(450 + 49r)(aa_2 - aa_1) + \\ +Pe(241aa_3 + 241aa_4 - 16aa_1 - 16aa_2)\end{array}\right]}{\left[\begin{array}{c}(192r + 768Pe^2)(aa_1 + aa_2 - aa_3 - aa_4) + \\ +r^2(16aa_1 + 16aa_2 + 53aa_3 + 53aa_4) + 552Per(aa_1 - aa_2)\end{array}\right]}, \\
\zeta_{r_2} &= 16.875\frac{\left[\begin{array}{c}(40r + 160Pe^2)(aa_1 + aa_2 - aa_3 - aa_4) + \\ +r^2(4aa_1 + 4aa_2 + aa_3 + aa_4) + 40rPe(aa_1 - aa_2)\end{array}\right]}{\left[\begin{array}{c}(192r + 768Pe^2)(aa_1 + aa_2 - aa_3 - aa_4) + \\ +r^2(16aa_1 + 16aa_2 + 53aa_3 + 53aa_4) + 552Per(aa_1 - aa_2)\end{array}\right]},
\end{aligned}
\tag{B1}
$$

$$
aa_1 = e^{Pe + 0.5\sqrt{Pe^2 + r}}, \quad aa_2 = e^{0.5\sqrt{Pe^2 + r}}, \quad aa_3 = e^{0.5Pe + \sqrt{Pe^2 + r}}, \quad aa_4 = e^{0.5Pe}
$$

$$\begin{aligned}\zeta_{a_1} = [&P_1(a_6^2e_3a_1 + e_5d_8^2a_4 - a_6^2a_3e_1 - a_5d_8^2e_4 + a_6e_5d_8a_1 + a_3a_7e_5d_8 + a_6e_3a_4d_8 - e_3a_7a_5d_8\\ &- a_6a_3e_4d_8 - a_6a_5d_8e_1) + P_2(e_5d_8^2a_2 - a_5d_8^2e_2 - a_6a_3a_7e_1 + a_1a_7e_5d_8 + a_6e_3a_2d_8\\ &- a_5d_8a_7e_1 + a_6e_3a_7a_1 - a_6a_3e_2d_8) + P_3(-a_6a_3e_2d_8 - a_6a_3a_7e_1 + a_6e_3a_2d_8\\ &+ a_6e_3a_7a_1 + e_5d_8a_7a_1 - a_5d_8a_7e_1 + e_5d_8^2a_2 - a_5d_8^2e_2) + P_4(-e_1a_7^2a_3 - a_4d_8^2e_2\\ &+ e_4d_8^2a_2 + a_7^2e_3a_1 - a_4d_8a_7e_1 - a_7a_3e_2d_8 + e_4d_8a_7a_1 + a_7e_3a_2d_8 - a_6a_1e_2d_8\\ &+ a_6e_1a_2d_8)]/[P_1(-a_7b_3e_5d_8 - a_6b_1e_5d_8 + b_5d_8a_6e_1 + b_5d_8a_7e_3 - b_4d_8^2e_5\\ &- a_6^2b_1e_3 + b_5d_8^2e_4 + a_6^2b_3e_1 - b_4d_8a_6e_3 + a_6b_3e_4d_8) + P_2(a_7b_3a_6e_1 + e_2d_8a_6b_3\\ &- a_6b_1a_7e_3 + e_1a_7b_5d_8 - b_1a_7e_5d_8 - b_2d_8^2e_5 + e_2d_8^2b_5 - b_2d_8a_6e_3) + P_3(-b_1a_7e_5d_8\\ &- a_6b_1a_7e_3 + e_2d_8a_6b_3 + e_1a_7b_5d_8 + a_7b_3a_6e_1 - b_2d_8^2e_5 + e_2d_8^2b_5 - b_2d_8a_6e_3)\\ &+ P_4(-b_2d_8a_7e_3 - b_1a_7e_4d_8 + e_2d_8a_7b_3 + e_2d_8a_6b_1 + e_1a_7b_4d_8 - b_2d_8a_6e_1\\ &+ e_1a_7^2b_3 - b_1a_7^2e_3 + e_2d_8^2b_4 - b_2d_8^2e_4)],\end{aligned} \tag{B2}$$

$$\begin{aligned}\zeta_{r_1} = -[&P_1(-b_4d_8a_6a_3 + b_5d_8a_6a_1 - a_7b_3a_5d_8 - a_6b_1a_5d_8 + b_5d_8a_7a_3 - a_6^2b_1a_3 - b_4d_8^2a_5\\ &+ a_6^2b_3a_1 + b_5d_8^2a_4 + a_6b_3a_4d_8) + P_2(a_1a_7b_5d_8 - b_1a_7a_5d_8 - b_2d_8a_6a_3 - a_6b_1a_7a_3\\ &+ a_2d_8a_6b_3 + a_7b_3a_6a_1 - b_2d_8^2a_5 + a_2d_8^2b_5) + P_3(a_2d_8^2b_5 - b_2d_8^2a_5 + a_2d_8a_6b_3\\ &- b_2d_8a_6a_3 + a_1a_7b_5d_8 - a_6b_1a_7a_3 - b_1a_7a_5d_8 + a_7b_3a_6a_1) + P_4(-b_2d_8a_7a_3 + a_2d_8a_6b_1\\ &+ a_2d_8a_7b_3 - b_1a_7a_4d_8 + a_1a_7b_4d_8 - b_2d_8a_6a_1 + a_1a_7^2b_3 - b_1a_7^2a_3 - b_2d_8^2a_4\\ &+ a_2d_8^2b_4)]/[P_1(-a_7b_3e_5d_8 - a_6b_1e_5d_8 + b_5d_8a_6e_1 + b_5d_8a_7e_3 - b_4d_8^2e_5 - a_6^2b_1e_3\\ &+ b_5d_8^2e_4 + a_6^2b_3e_1 - b_4d_8a_6e_3 + a_6b_3e_4d_8) + P_2(a_7b_3a_6e_1 + e_2d_8a_6b_3 - a_6b_1a_7e_3\\ &+ e_1a_7b_5d_8 - b_1a_7e_5d_8 - b_2d_8^2e_5 + e_2d_8^2b_5 - b_2d_8a_6e_3) + P_3(-b_1a_7e_5d_8 - a_6b_1a_7e_3\\ &+ e_2d_8a_6b_3 + e_1a_7b_5d_8 + a_7b_3a_6e_1 - b_2d_8^2e_5 + e_2d_8^2b_5 - b_2d_8a_6e_3) + P_4(-b_2d_8a_7e_3\\ &- b_1a_7e_4d_8 + e_2d_8a_7b_3 + e_2d_8a_6b_1 + e_1a_7b_4d_8 - b_2d_8a_6e_1 + e_1a_7^2b_3 - b_1a_7^2e_3\\ &+ e_2d_8^2b_4 - b_2d_8^2e_4)],\end{aligned}$$

$$P_1 = e^{2Pe+\sqrt{Pe^2+r}}, \quad P_2 = e^{Pe+2\sqrt{Pe^2+r}}, \quad P_3 = e^{Pe}, \quad P_4 = e^{\sqrt{Pe^2+r}}.$$